ASTRONOMY & ASTROPHYSICS
SUPPLEMENT SERIES

Astron. Astrophys. Suppl. Ser. **133**, 257–269 (1998)

Recombination coefficients for Ne II lines at nebular temperatures and densities⋆

R. Kisielius[1], P.J. Storey[1], A.R. Davey[2], and L.T. Neale[1]

[1] Department of Physics and Astronomy, University College London, Gower Street, London WC1E 6BT, UK
[2] Department of Physics, Montana State University, Bozeman, MT 59717-3840, U.S.A.

Received May 25; accepted June 9, 1998

Abstract. We calculate total recombination coefficients for $Ne^{2+} + e^-$ and effective recombination coefficients for the formation of selected lines of Ne II. New photoionization data are calculated which accurately map the near threshold resonances and are used to derive recombination coefficients for principal quantum numbers, $n \leq 15$, including radiative and dielectronic recombination. Cascading from higher states is included, allowing for the effects of finite electron density in a hydrogenic approximation. The effects of population in the excited states of the recombining ion are investigated.

Key words: atomic data — H II regions — planetary nebulae: general

1. Introduction

The principal means of determining elemental abundances in nebular plasmas has, until recently, been from the measurement of collisionally excited optical forbidden lines. The emissivities of these lines are very sensitive to the electron temperature at the temperatures typical of photoionized nebulae. An alternative method of determining abundance is to ratio the intensities of recombination lines with those of hydrogen. Such ratios are only weakly dependent on temperature. Abundances of C , N and O derived from recombination lines are, however, larger than those derived from forbidden lines by factors ranging from 2 to 10 (e.g. Liu et al. 1995). The origin of these differences is at present unexplained. The prerequisite for determination of recombination line abundances is reliable recombination coefficients for atomic ions. In this paper we present new recombination coefficients for the formation of lines of Ne II.

Recombination coefficients for Ne II ions have been given by Péquignot et al. (1991) considering only radiative recombination. Nussbaumer & Storey (1987) tabulated dielectronic recombination coefficients for Ne II obtained from a model in which resonance states are represented by bound-state wave functions. We follow the approach of Storey (1994) who, for recombination to O II, used a unified approach to the treatment of radiative and dielectronic recombination by calculating recombination coefficients directly from photoionization cross-sections for each initial state. A new calculation of photoionization cross-sections is carried out using the ab initio methods developed for the Opacity Project (Seaton 1987; Berrington et al. 1985) and the Iron Project (Hummer et al. 1993), hereafter referred to only as OP methods. These calculations employ the R-matrix formulation of the close-coupling method, and the resulting cross-sections are expected to be of high quality. The existing photoionization data for Ne II states deposited in the Opacity Project database (Cunto et al. 1993) is inadequate for our purposes, as explained more fully below. Transition probabilities for all low-lying bound states are also calculated using the same method, so that the bound-bound and bound-free radiative data used here are expected to be significantly more accurate than those used by previous authors.

The effects of finite electron density are also incorporated, using the methods described by Hummer & Storey (1987) for hydrogenic ions, but the treatment is not complete and the results are only applicable to plasmas of relatively low electron density. The range of validity is discussed more fully in Sect. 4.1. The process of high temperature dielectronic recombination originally described by Burgess (1964) is not included in the present calculations, so the results are only appropriate for relatively low electron temperatures, $T \leq 27\,000$ K (Nussbaumer & Storey 1983). The temperature and density range are nonetheless

Send offprint requests to: P.J. Storey

⋆ All tables are available in electronic form at the CDS via anonymous ftp to cdsarc.u-strasbg.fr (130.79.128.5) or via http://cdsweb.u-strasbg.fr/Abstract.html

sufficient for the analysis of the spectra of nebular objects; planetary nebulae, H II regions and nova shells.

2. Atomic data for Ne^+

2.1. The Ne^+ *term scheme*

The principal series of Ne II is $2s^22p^4\,(^3P)nl$, which gives rise to doublet and quartet terms. Also interspersed among the bound states are members of the series $2s^22p^4\,(^1D)nl$ and $2s^22p^4/(^1S)nl$, which only give rise to doublet terms. The latter two series also have members lying above the first ionization limit, which appear as resonances in the photoionization of the true bound states and hence may give rise to low-temperature dielectronic recombination.

The tables of Nussbaumer & Storey (1984), show that this process mainly affects the two doublet terms in the ground electronic configuration, $2s^22p^5$ ($^2D^o$, $^2P^o$). The calculation of recombination coefficients and the role of dielectronic recombination are discussed in Sect. 2.5.

We use the OP methods to calculate the bound-bound and bound-free radiative data for Ne II assuming LS-coupling. Consequently, there are no radiative transitions between quartet and doublet states. The data extend up to principal quantum number $n = 15$ and to total atomic orbital angular momentum quantum number $L = 6$. We therefore partition the calculation of level populations into several distinct regimes, according to quantum numbers and energy. We define E_0 as the ionization energy in the principal series of Ne^+ corresponding to $n = 15$; ($E_0 = 0.0178$ Ry).

We also define the principal quantum number $n = n_d$, such that for $n < n_d$, the population structure is determined solely by radiative processes. Collisionally induced transitions can be neglected. The approximations that are used for different values of n are described fully in Storey (1994). We give only a brief summary here.

(1) $n > n_d$: The rate of l-changing collisions is more rapid than the rate of radiative decay. Populations in this regime are taken from a purely hydrogenic calculation of departure coefficients, b_{nl}, using the method described by Hummer & Storey (1987), which makes full allowance for all collisional effects. Only states that belong to the principal series of Ne^+ are included.

(2) $15 < n \leq n_d$: Collisional effects are no longer important, so populations are now determined only by radiative processes, but no accurate atomic data are available. Various approximate methods are used to calculate energy levels, radiative transition probabilities and recombination coefficients. Only states that belong to the principal series of Ne^+ are included.

(3) States with ionization energy less than or equal to E_0: All atomic terms in this energy regime are included in the calculation of populations, irrespective of parentage.

Table 1. Comparison of calculated and experimental energies (in Ry) for the Ne^{2+} target states

Configuration	Term	present	experimental
$1s^22s^22p^4$	^3P	0.00000	0.00000
	^1D	0.24342	0.23257
	^1S	0.50909	0.50512
$1s^22s2p^5$	^3P	1.86189	1.86142
	^1P	2.63502	2.68209
$1s^22p^6$	^1S	4.39958	4.36048

An energy ordered list of terms is set up and it is assumed that their populations are determined solely by recombination and radiative cascading from all accessible higher states.

2.2. New R-matrix calculation

We have carried out a new calculation of bound state energies, oscillator strengths and photoionization cross-sections for Ne II states with $n \leq 15$ using the suite of programmes developed for the Opacity Project (Seaton 1987; Berrington et al. 1985) and the Iron Project (Hummer et al. 1993). The Ne^{2+} target state wave functions were calculated with the general purpose atomic structure code SUPERSTRUCTURE (Eissner et al. 1974) with the modifications of Nussbaumer & Storey (1978). The wave functions of the six target terms were expanded in terms of the electron configurations $1s^22s^22p^4$, $1s^22s2p^5$, $1s^22p^6$, $1s^22s^22p^3\bar{3}l$, $1s^22s2p^4\bar{3}l$, $1s^22p^5\bar{3}l$, $1s^22s^22p^2\bar{3}l\bar{3}l'$, $1s^22s2p^3\bar{3}l\bar{3}l'$, $1s^22p^4\bar{3}l\bar{3}l'$, where 1s, 2s and 2p are spectroscopic orbitals and $\bar{3}l$, $\bar{3}l'$ ($l, l' = 0, 1, 2$) are correlation orbitals. The one-electron radial functions were calculated in adjustable Thomas-Fermi potentials, with the potential scaling parameters λ_{nl} determined by minimising the sum of the energies of six target states. In our case, we obtained for the scaling parameters: $\lambda_{1s} = 1.45892$, $\lambda_{2s} = 1.12996$, $\lambda_{2p} = 1.08051$, $\lambda_{\bar{3}s} = -1.01396$, $\lambda_{\bar{3}p} = -0.94108$, $\lambda_{\bar{3}d} = -1.14250$, with the negative values having the significance detailed by Nussbaumer & Storey (1978).

In Table 1, we compare experimental target state energies with our calculated values. We use the experimental values for the target energies to obtain the Hamiltonian matrix of the $(N + 1)$ electron system in our calculation of energy levels, oscillator strengths and photoionization cross-sections of Ne II.

2.3. Energy levels

Experimental energy levels for Ne^+ have been given by Persson (1971) for members of the series $2s^22p^4$ (^3P, ^1D, ^1S)nl with $n \leq 9$ and $l \leq 4$, although some levels are

missing. For states where no data are given by Persson, energies have been estimated in the following ways.

Our new calculation of energy levels includes all terms $2s^p2p^q$ (S_cL_c) nl (SL) with ionization energy less than E_0 and $L \leq 6$, where S_c and L_c are the total angular momentum quantum numbers of the core electrons. Energies calculated by ab initio methods have been used in preference to quantum defect extrapolation from experimentally known lower terms because they allow, albeit approximately, for the presence of perturbations of the principal series by members of other series. Such perturbations can significantly alter energy levels and the radiative properties of the states.

Secondly, for states with $15 < n \leq n_d$, and $l \leq 5$, where calculated energies exist for lower members of the series, a quantum defect has been calculated for the highest known member (usually with $n = 15$), and this quantum defect has been used to determine the energies of all higher terms.

Finally, if neither of the above methods can be used, the term is assumed to have hydrogenic energy.

2.4. Bound-bound radiative data

Radiative transition probabilities are taken from three sources:

(1) Ab initio calculation: We have computed values of (gf) for all the bound terms with ionization energy less than or equal to E_0, and with $L \leq 6$. The data are in LS-coupling and in the electric dipole approximation, so there are no transitions between states of different total spin, but two-electron transitions, which involve a change of core state are included.

(2) Coulomb approximation: For pairs of terms which were not computed by the method described in (1), but where one or both of the states have a non-zero quantum defect, the dipole radial integrals required for the calculation of transition probabilities are calculated using the Coulomb approximation. Details are given in Storey (1994).

(3) Hydrogenic approximation: For pairs of terms with zero quantum defect hydrogenic dipole radial integrals are calculated, either using the expressions of Gordon (1929) in terms of hypergeometric functions, or using direct recursion on the matrix elements themselves as described by Storey & Hummer (1991). More details on determining transition probabilities were presented by Storey (1994).

2.5. Photoionization cross-sections and recombination coefficients

The recombination coefficient for each term SL, or orbital nl is calculated directly from the photoionization cross-section for that state. As in the bound-bound case, there are three approximations in which the photoionization data are obtained.

(1) Photoionization cross-sections were computed for all terms with ionization energy less than or equal to E_0 and $L \leq 5$. In general, the cross-section for each state consists of a background contribution which declines monotonically with increasing ejected electron energy, and resonance contributions. These cross-sections can in principle be convolved with a thermal distribution of free-electron energies to obtain a recombination coefficient which incorporates both "radiative" and "dielectronic" recombination. There are two potential problems with this approach. The first is a shortcoming of the theory, in that the photoionization cross-sections have been calculated using first-order perturbation theory. This approach does not give the correct behaviour of the cross-section in the vicinity of a resonance whose radiative width is greater than its autoionization width (Seaton & Storey 1976), and overestimates the contribution of such a resonance to the recombination coefficient. This problem can only be overcome in general by including radiative channels in the original scattering calculation (Bell & Seaton 1985), and this cannot yet be done for complex ions. We discuss this problem further in Sect. 2.6 below.

The second problem is that in many cases treated in the OP, the free-electron energy mesh on which the cross-section was calculated was too coarse to accurately describe the narrower resonance features. The contribution of a resonance to the recombination coefficient depends on the area under it, which is also a measure of the oscillator strength between the initial state and the resonance. The width of a resonance, however, depends on the strength of the interaction with the accessible continuum states, and is independent of the area under it. As a result, a resonance may contribute significantly to the recombination to a particular state, but still be very narrow. Such resonances may be poorly described or missed altogether by calculation on a coarse energy mesh. We discuss the treatment of this problem further in Sect. 2.6 below.

(2) Coulomb approximation: As in the bound-bound case, the Coulomb approximation is used for terms where no OP data is available, but which have a non-zero quantum defect. The calculation of photoionization cross-section data using Coulomb functions has been described by Burgess & Seaton (1960) and Peach (1967), whose tables are used here.

(3) For the remaining states, hydrogenic photoionization cross-sections are used, calculated using the methods and computer codes of Storey & Hummer (1991).

2.6. Energy mesh for Ne II *photoionization cross-sections*

In many cases treated by the OP, the free electron energy mesh on which the photoionization cross-sections are calculated, was too coarse to accurately map narrow resonance features. The photoionization cross-sections for Ne II generated by the OP were based on a quantum

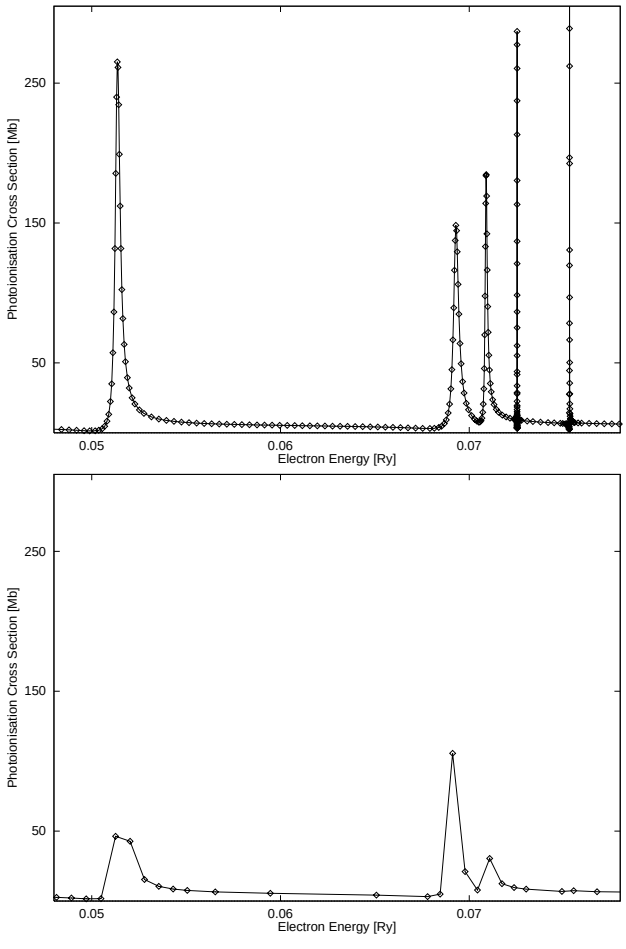

Fig. 1. Comparison of the photoionization cross-section (in Mb) for the ground state $2s^2 2p^5\ ^2P^o$ of Ne II calculated in this work (top) and by the OP (bottom)

defect mesh with 100 points per unit increase in the effective quantum number derived from the next threshold. Figure 1 (bottom) shows a section of the OP cross-section from the ground state of Ne II (Cunto et al. 1993), in which resonance peaks are truncated by the coarse mesh.

In contrast to the OP calculations, we use a variable step energy mesh for photoionization cross-sections that delineates all resonances to a prescribed accuracy. The first step is to employ quantum defect theory (Seaton 1983) to determine the positions and widths of all resonances in a specific energy region. Since the quantum defect methods rely on functions that vary slowly with electron energy, only a coarse energy mesh is required for this step. Resonances are due to poles in the scattering matrix $\mathcal{S}$ described by a matrix χ which varies slowly with energy and contains functions pertaining to both open (o) and closed (c) channels:

$$\mathcal{S} = \chi_{oo} - \chi_{oc}\left[\chi_{cc} - \exp(-2\pi i\nu)\right]^{-1}\chi_{co}. \quad (1)$$

Diagonalization of the matrix χ_{cc} yields the complex effective quantum numbers, ν related to the complex quantum defect μ_c

$$\mu_c = \alpha + i\beta \quad (2)$$

by $\nu = n - \mu_c$. The complex energy of the $\mathcal{S}$ matrix pole $\varepsilon(\text{pole})$ is related to α and β by

$$\varepsilon(\text{pole}) = \varepsilon_c - (n-\alpha)^{-2} - \frac{i}{2}\gamma, \quad (3)$$

where $\gamma = 4\beta\,(n-\alpha)^{-3}$ is the autoionization width of resonance and ε_c is the appropriate target energy.

In the second step, we determine a new fine energy mesh of variable step length $\Delta\varepsilon$ assuming a Lorentzian profile for each resonance:

$$F(\varepsilon,\gamma) = \frac{\left(\frac{\gamma}{2}\right)^2}{\left(\varepsilon - \varepsilon(\text{pole})\right)^2 + \left(\frac{\gamma}{2}\right)^2}. \quad (4)$$

To calculate recombination coefficients, we integrate the photoionization cross-sections using a 3-point Simpson's rule. If we specify the accuracy required for each three-point integration as Δ, we can find the necessary energy interval for a given resonance from the known error associated with Simpson's rule

$$\Delta\varepsilon = \frac{90\Delta}{F^{(4)}(\xi)}, \quad (5)$$

where $F^{(4)}(\xi)$ is the maximum value of the 4th derivative of the Lorentzian function in the given interval. This leads to an iterative procedure in which the step length and the fourth derivative are recalculated until the integration error over the next two points is below the specified value. It is repeated for all the resonances and the smallest value of $\Delta\varepsilon$ obtained is used for the next two steps.

Such detailed consideration of the energy mesh was undertaken for the regions from the $2s^2 2p^4(^3P)$ limit up to 0.0178 Ry below the $2s^2 2p^4(^1D)$ limit and from the $2s^2 2p^4(^1D)$ limit up to 0.0178 Ry below the $2s^2 2p^4(^1S)$ limit, since these regions contain the main contribution to the recombination at the temperatures of interest. The energy 0.0178 Ry corresponds to a principal quantum number of fifteen relative to the next threshold. In the region above the $2s^2 2p^4(^1S)$ threshold, a quantum defect mesh was used.

One problem that arose was that of interlopers from higher series. In the region below a particular threshold, the quantum defect method outlined above does not give information about resonances that come from higher thresholds, these having been eliminated by the use of contracted matrices (Seaton 1983). Below the (^{1}D) threshold and in the range of our variable step energy mesh calculation, there are resonances arising from the (^{1}S)3d ^{2}P, ^{2}S and (^{1}S)3p ^{2}P^o states. The positions and widths of these resonances were determined from a preliminary calculation of photoionization cross-sections from a suitable bound state. These data were then added to the list of

resonance information used to generate the final energy mesh for the detailed photoionization calculations.

In Fig. 1, we demonstrate the difference in resolution between the OP cross-section (Cunto et al. 1993) and the one calculated by our method for the ground state ^{2}P^o of Ne II. The OP cross section in the energy region between the first and second ionization threshold consists of 124 points based on a quantum defect mesh whilst the latter is based on an energy mesh of 2600 points. In the OP cross-section, the resonances are usually described by three or four points, and some of them are missing altogether. As one can also see from Fig. 1, there is also a significant difference in the peak heights of the resonances between the two calculations.

These differences lead to a significant change in the calculated area under the two cross-sections leading in turn to a difference in the derived recombination coeffcients. In the above case, the area under the OP curve is about 15% smaller than is obtained from our data. This difference becomes even more pronounced when we consider only the area under particular resonances removing the effect of the background. In the case of the low-lying resonance at $\varepsilon = 0.0514$ Ry which is very significant in determining the recombination coefficient, the area under our cross-section is 0.130 Mb · Ry whereas the OP data give 0.085 Mb · Ry. The importance of the correct delineation of resonances is greatest for recombination to states whose parent is an excited state of Ne^{2+}, since their photoionization cross-sections generally have little or no background contribution.

The unified approach suffers from a shortcoming whereby, the cross-section in the vicinity of resonance whose autoionization width is comparable or smaller than its radiative width overestimates its contribution to the recombination coefficient. To address this problem of radiative damping of resonances, we have compared total radiative decay probabilities (calculated with SUPERSTRUCTURE) with autoionization probabilities calculated with the quantum defect methods described above. As a result, the resonances corresponding to the states $2s^22p^4(^1D)nf,ng$ (^2L, $L > 3$) were eliminated from the list of resonances used to generate the energy mesh. As a result, a coarse energy mesh was used in the vicinity of these very narrow reonances and they were absent from the calculated photoionization cross-section.

3. Calculation of Ne^+ populations

3.1. The Ne^+ *populations*

The calculation of the population structure is a two-stage process. The first stage involves the calculation of a purely hydrogenic model to determine the departure coefficients b_{nl}, related to the populations N_{nl} by

$$\left(\frac{N_{nl}}{N_e N_+}\right) = \left(\frac{N_{nl}}{N_e N_+}\right)_S b_{nl}, \quad (6)$$

where the subscript S refers to the value of the ratio given by the Saha equation, and N_e and N_+ are the number densities of electrons and recombining ions respectively. The details of the atomic rate coefficients and the numerical techniques employed in this calculation have been fully described elsewhere (Hummer & Storey 1987, 1992).

The second stage starts from the hydrogenic results for $n > n_d$, and then solves for the populations of the states from $n = n_d$ to $n = 16$ in descending order. The populations of states with $n \leq 15$ are determined by matrix inversion. More details are given by Storey (1994).

3.2. The Cases A and B

Baker & Menzel (1938) defined the Cases A and B with reference to the recombination spectrum of hydrogen. In Ne II, there is only one low-lying term, $2s^22p^5\ ^2P^o$. Accordingly, two cases can be defined for Ne II. In Case A, all emission lines are assumed to be optically thin. In Case B, lines terminating on the $^2P^o$ term are assumed to be thick and no radiative decays to this state are permitted when calculating the population structure. Since the calculations are made entirely in *LS*-coupling, Cases A and B differ only for the doublet series.

4. Results and discussion

4.1. Total and effective recombination coefficients

The population structure of Ne^+ has been calculated for the electron temperatures T_e = 1000, 2000, 3000, 5000, 7500, 10 000, 12 500, 15 000, 20 000 K, and for the electron densities $N_e = 10^2$, 10^4, 10^5, 10^6 cm^{-3}. For electron densities greater than 10^6 cm^{-3}, l-changing collisions would have to be included for $n < 15$, which is beyond the scope of the current approximation.

In Table 2, we give the total recombination coefficients for $Ne^{2+} + e^-$ for the above range of electron temperatures and densities. Total recombination coefficients were obtained by summing recombination coefficients to the metastable and ground states of Ne^+.

In Tables 3 and 4 are given the effective recombination coefficients $\alpha_{eff}(\lambda)$, for the strongest recombination lines of Ne II. The effective recombination coefficient is defined such that the emissivity $\epsilon(\lambda)$, in a transition of wavelength λ is

$$\epsilon(\lambda) = N_e N_+ \alpha_{eff}(\lambda)\frac{hc}{\lambda} \quad [\mathrm{erg\,cm^{-3}\,s^{-1}}]. \quad (7)$$

Results are not tabulated for $N_e = 10^2$ cm^{-3} and $N_e = 10^5$ cm^{-3} as the recombination coefficients are not significantly different to those at 10^4 cm^{-3}; typically they agree within two percent. In the tables, data are given for Cases A and B, as appropriate, but data for Case B are tabulated only if the recombination coefficients differ by more than

Table 2. Total recombination coefficients [10^{-12} cm^3 s^{-1}]

		log(N_e)			
T[K]	Case	2	4	5	6
1000	A	7.40	7.72	8.15	9.00
	B	6.06	6.33	6.70	7.45
2000	A	4.62	4.70	4.82	5.05
	B	3.67	3.73	3.82	4.02
3000	A	3.56	3.60	3.65	3.75
	B	2.75	2.77	2.81	2.90
5000	A	2.61	2.62	2.64	2.68
	B	1.91	1.91	1.92	1.95
7500	A	2.03	2.04	2.04	2.06
	B	1.41	1.41	1.41	1.43
10 000	A	1.69	1.69	1.70	1.71
	B	1.14	1.13	1.13	1.14
12 500	A	1.46	1.46	1.46	1.47
	B	0.95	0.95	0.95	0.95
15 000	A	1.29	1.29	1.29	1.29
	B	0.82	0.82	0.82	0.82
20 000	A	1.05	1.05	1.05	1.06
	B	0.65	0.65	0.64	0.65

one percent from the Case A values. Also tabulated is the air wavelength of the multiplet, which is calculated from the centres of gravity of the two terms involved. Most of the multiplets listed have considerable fine-structure and the reader is referred to Persson (1971) for a full list of fine-structure transitions and their wavelengths, although we tabulate the relative strengths and wavelengths of some of the strongest transitions (see Sect. 4.2 below). Transitions are included in the tables according to the following criteria:

(1) All the components of the 3d–3p and 3p–3s transition arrays are given irrespective of intensity, including those with ^{1}D and ^{1}S parentage. These transitions fall in the visible part of the spectrum and among them are the strongest recombination lines of Ne II.

(2) For other transition arrays, only transitions with effective recombination coefficients greater than 10^{-14} cm^3 s^{-1} at at least one temperature are tabulated. However, we did not include transitions having $l > 2$ because the LS-coupling scheme becomes inappropriate for such transitions.

(3) Only transitions giving rise to lines with wavelengths greater than 91.2 nm are tabulated.

In Table 5, fit parameters and maximum deviations from the calculated data are given for the effective recombination coefficients at $N_e = 10^4$ cm^{-3}. The coefficients are fitted by a least-squares algorithm to the functional form

$$\alpha_{\rm eff} = 10^{-14}\, a t^f \left(1 + b\,(1-t) + c\,(1-t)^2 + d\,(1-t)^3\right), \quad (8)$$

where $t = T_e[\mathrm{K}]/10^4$, and a, b, c, d and f are constants. Fitting is valid for the whole temperature range studied for all lines except those denoted by asterisk in the last column.

One can notice that the fits are typically accurate to within a few tenths of one percent for all lines in the main series, with the exception being the lines originating from the 4p (^{2}P^o) and 3p (^{2}P^o) states. Here we have a maximum fitting error $< 2\%$. The fitting of the lines from the second and third series (denoted by an asterisk) is valid for the temperature range $T_e = 2000 - 20\,000$ K, and the fitting error is typically within 1.5% and not exceeding 3.5%. For these lines, direct radiative recombination and dielectronic recombination are of equal importance at low temperatures. For this reason, the effective recombination coefficients have a more complex dependence on temperature.

The value of parameter a is constrained to have the value of $10^{14}\alpha_{\rm eff}(\lambda)$ at $t = 1$. An approximate fit to the effective recombination coefficients at a different value of N_e can be obtained by replacing a with $\alpha_{\rm eff}(\lambda, t = 1)$ at that density.

4.2. Relative line strengths

To get the effective line recombination coefficient for the transitions between the initial level SL_iJ_i and the final level SL_fJ_f of the multiplet $SL_i - SL_f$, one should use the relation

$$\alpha_{\rm eff}\,(SL_iJ_i \to SL_fJ_f) = \alpha_{\rm eff}\,(SL_i \to SL_f)\, b(J_i, J_f), \quad (9)$$

where the factors $b(J_i, J_f)$ can be calculated using the expression

$$b(J_i, J_f) = \frac{(2J_i+1)(2J_f+1)}{(2S+1)} \left\{ \begin{array}{cccc} J_i & J_f & 1 \\ L_f & L_i & S \end{array} \right\}^2, \quad (10)$$

where { } is the six-j symbol defined, for example, by Brink & Satchler (1968).

Values of $\alpha_{\rm eff}\,(SL_i \to SL_f)$ may be obtained either from Tables 3 and 4 or by using Eq. (8) and data from Table 5. In Table 6, we tabulate the factors $b(J_i, J_f)$ and wavelengths of lines in the strongest multiplets of Ne II. The multiplets were chosen to satisfy the condition that their effective recombination coefficients are greater than 10^{-13} cm^3 s^{-1} at temperature 5000 K. Only transitions within the 3d–3p and 3p–3s arrays having ^{3}P parentage fulfil this condition.

The air wavelengths of the transitions presented in Table 6 were taken from Persson (1971).

4.3. Population of excited states of Ne^{2+}

In most calculations of recombination coefficients in nebular plasmas it is assumed that only the ground state of

Table 5. Fitting coefficients and maximum fitting errors (%) for effective recombination coefficients. Electron density $N_e = 10^4$ [cm^{-3}]. Asterisks denote lines for which fitting is valid from $T_e = 2000$ K

Transition	λ[nm]	Case	a	b	c	d	f	%
7d (^{4}F^e) – 7p (^{4}D^o)	5790.2	A	0.279	−0.870	−0.096	−0.022	−1.5770	0.09
		B	0.281	−0.893	−0.083	−0.014	−1.6000	0.05
6d (^{4}F^e) – 6p (^{4}D^o)	3527.9	A	0.637	−0.876	−0.092	−0.022	−1.6047	0.09
		B	0.641	−0.896	−0.081	−0.015	−1.6255	0.04
6d (^{4}D^e) – 6p (^{4}P^o)	3435.0	A	0.344	−0.862	−0.101	−0.023	−1.5359	0.09
		B	0.345	−0.887	−0.088	−0.014	−1.5606	0.05
6d (^{2}F^e) – 6p (^{2}D^o)	3673.1	A	0.348	−0.867	−0.099	−0.024	−1.6019	0.10
		B	0.355	−0.888	−0.088	−0.016	−1.6221	0.04
6d (^{4}F^e) – 5p (^{4}D^o)	922.7	A	0.370	−0.876	−0.092	−0.022	−1.6053	0.09
		B	0.372	−0.896	−0.081	−0.015	−1.6257	0.04
6d (^{4}F^e) – 4p (^{4}D^o)	372.6	A	0.237	−0.876	−0.092	−0.022	−1.6049	0.09
		B	0.239	−0.896	−0.081	−0.015	−1.6254	0.04
6p (^{4}D^o) – 5d (^{4}F^e)	3760.7	A	0.277	−0.875	−0.086	−0.028	−1.5758	0.12
		B	0.279	−0.901	−0.072	−0.019	−1.6016	0.04
6p (^{4}D^o) – 3s (^{4}P^e)	104.1	A	0.306	−0.875	−0.086	−0.027	−1.5760	0.11
		B	0.308	−0.901	−0.072	−0.019	−1.6015	0.04
6p (^{4}P^o) – 3s (^{4}P^e)	104.4	A	0.357	−0.865	−0.093	−0.028	−1.5329	0.13
		B	0.360	−0.894	−0.077	−0.018	−1.5621	0.04
5d (^{4}F^e) – 5p (^{4}D^o)	1871.3	A	1.723	−0.888	−0.085	−0.020	−1.6472	0.07
		B	1.731	−0.900	−0.078	−0.016	−1.6598	0.04
5d (^{4}D^e) – 5p (^{4}D^o)	1963.1	A	0.275	−0.857	−0.104	−0.025	−1.5568	0.10
		B	0.276	−0.881	−0.092	−0.017	−1.5798	0.05
5d (^{4}D^e) – 5p (^{4}P^o)	1802.0	A	0.979	−0.857	−0.104	−0.025	−1.5568	0.10
		B	0.984	−0.881	−0.092	−0.017	−1.5801	0.05
5d (^{4}P^e) – 5p (^{4}S^o)	2092.7	A	0.335	−0.843	−0.114	−0.030	−1.5583	0.11
		B	0.337	−0.867	−0.101	−0.021	−1.5826	0.05
5d (^{2}F^e) – 5p (^{2}D^o)	2004.9	A	0.879	−0.877	−0.093	−0.022	−1.6414	0.09
		B	0.902	−0.891	−0.085	−0.017	−1.6545	0.04
5d (^{2}D^e) – 5p (^{2}P^o)	2413.8	A	0.005	−0.820	−0.132	−0.032	−1.5478	0.11
		B	0.250	−0.847	−0.119	−0.019	−1.5650	0.03
5d (^{4}F^e) – 4p (^{4}D^o)	468.6	A	0.762	−0.888	−0.085	−0.020	−1.6474	0.07
		B	0.766	−0.900	−0.078	−0.016	−1.6596	0.04
5d (^{4}D^e) – 4p (^{4}P^o)	453.2	A	0.435	−0.857	−0.105	−0.025	−1.5564	0.10
		B	0.437	−0.881	−0.092	−0.017	−1.5797	0.05
5d (^{2}F^e) – 4p (^{2}D^o)	480.8	A	0.356	−0.877	−0.093	−0.022	−1.6418	0.08
		B	0.365	−0.891	−0.085	−0.017	−1.6542	0.04
5p (^{4}D^o) – 5s (^{4}P^e)	2491.6	A	0.585	−0.886	−0.080	−0.024	−1.6105	0.09
		B	0.589	−0.905	−0.070	−0.018	−1.6294	0.03
5p (^{4}P^o) – 5s (^{4}P^e)	2810.5	A	0.275	−0.863	−0.095	−0.028	−1.5455	0.12
		B	0.278	−0.891	−0.079	−0.018	−1.5739	0.05
5p (^{2}D^o) – 5s (^{2}P^e)	2577.8	A	0.226	−0.883	−0.082	−0.025	−1.6186	0.10
		B	0.273	−0.896	−0.078	−0.017	−1.6246	0.03
5p (^{4}D^o) – 4d (^{4}F^e)	1990.3	A	0.956	−0.886	−0.080	−0.024	−1.6102	0.09
		B	0.963	−0.905	−0.070	−0.018	−1.6295	0.03
5p (^{4}D^o) – 4d (^{4}D^e)	1782.9	A	0.203	−0.886	−0.080	−0.024	−1.6102	0.09
		B	0.204	−0.905	−0.070	−0.018	−1.6296	0.03
5p (^{4}P^o) – 4d (^{4}D^e)	1940.4	A	0.391	−0.863	−0.095	−0.028	−1.5458	0.12
		B	0.394	−0.891	−0.079	−0.018	−1.5738	0.05
5p (^{4}S^o) – 4d (^{4}P^e)	1904.5	A	0.273	−0.858	−0.097	−0.031	−1.5536	0.11
		B	0.275	−0.885	−0.082	−0.022	−1.5802	0.05
5p (^{2}D^o) – 4d (^{2}F^e)	1923.6	A	0.367	−0.884	−0.082	−0.025	−1.6190	0.10
		B	0.443	−0.896	−0.078	−0.017	−1.6250	0.03

Table 5. continued

Transition	λ[nm]	Case	a	b	c	d	f	%
5p (^{4}D^o) – 3d (^{4}F^e)	369.8	A	0.593	−0.886	−0.080	−0.024	−1.6101	0.09
		B	0.597	−0.905	−0.070	−0.018	−1.6294	0.03
5p (^{4}P^o) – 3d (^{4}D^e)	359.7	A	0.240	−0.863	−0.095	−0.028	−1.5457	0.12
		B	0.242	−0.892	−0.079	−0.018	−1.5739	0.05
5p (^{2}D^o) – 3d (^{2}F^e)	368.0	A	0.243	−0.884	−0.082	−0.025	−1.6188	0.10
		B	0.294	−0.896	−0.078	−0.017	−1.6246	0.03
5p (^{4}D^o) – 3s (^{4}P^e)	113.6	A	0.583	−0.886	−0.080	−0.024	−1.6101	0.09
		B	0.588	−0.905	−0.070	−0.018	−1.6297	0.03
5p (^{4}P^o) – 3s (^{4}P^e)	114.2	A	0.826	−0.863	−0.095	−0.028	−1.5458	0.12
		B	0.833	−0.892	−0.079	−0.018	−1.5740	0.05
5p (^{2}D^o) – 3s (^{2}P^e)	119.5	A	0.293	−0.884	−0.082	−0.025	−1.6187	0.10
		B	0.353	−0.895	−0.078	−0.018	−1.6243	0.03
5s (^{4}P^e) – 4p (^{4}P^o)	771.8	A	0.284	−0.890	−0.073	−0.026	−1.5856	0.11
		B	0.286	−0.913	−0.061	−0.019	−1.6079	0.04
5s (^{4}P^e) – 3p (^{4}D^o)	185.0	A	0.322	−0.890	−0.073	−0.026	−1.5854	0.11
		B	0.324	−0.913	−0.061	−0.019	−1.6081	0.04
5s (^{4}P^e) – 3p (^{4}P^o)	175.0	A	0.383	−0.890	−0.073	−0.026	−1.5855	0.11
		B	0.385	−0.913	−0.061	−0.019	−1.6081	0.04
4d (^{4}F^e) – 4p (^{4}D^o)	911.3	A	5.370	−0.871	−0.097	−0.027	−1.6720	0.11
		B	5.397	−0.880	−0.092	−0.023	−1.6826	0.08
4d (^{4}D^e) – 4p (^{4}D^o)	962.6	A	0.866	−0.852	−0.109	−0.029	−1.6033	0.12
		B	0.870	−0.871	−0.099	−0.022	−1.6221	0.06
4d (^{4}D^e) – 4p (^{4}P^o)	880.2	A	3.122	−0.852	−0.109	−0.029	−1.6036	0.12
		B	3.138	−0.871	−0.099	−0.022	−1.6221	0.06
4d (^{4}P^e) – 4p (^{4}D^o)	876.9	A	0.348	−0.840	−0.116	−0.032	−1.5913	0.12
		B	0.349	−0.860	−0.106	−0.025	−1.6110	0.06
4d (^{4}P^e) – 4p (^{4}P^o)	808.0	A	0.403	−0.840	−0.116	−0.033	−1.5907	0.12
		B	0.405	−0.861	−0.105	−0.025	−1.6113	0.05
4d (^{4}P^e) – 4p (^{4}S^o)	976.7	A	1.093	−0.840	−0.116	−0.032	−1.5912	0.12
		B	1.099	−0.860	−0.106	−0.025	−1.6110	0.06
4d (^{2}F^e) – 4p (^{2}D^o)	942.2	A	2.700	−0.862	−0.103	−0.028	−1.6678	0.12
		B	2.800	−0.874	−0.097	−0.023	−1.6768	0.08
4d (^{2}D^e) – 4p (^{2}D^o)	984.5	A	0.016	−0.776	−0.157	−0.045	−1.5519	0.16
		B	0.502	−0.801	−0.146	−0.034	−1.5660	0.06
4d (^{2}D^e) – 4p (^{2}P^o)	1221.2	A	0.029	−0.777	−0.157	−0.045	−1.5522	0.16
		B	0.887	−0.801	−0.146	−0.034	−1.5661	0.06
4d (^{2}P^e) – 4p (^{2}S^o)	947.1	A	0.050	−0.826	−0.136	−0.021	−1.5718	0.11
		B	0.531	−0.849	−0.123	−0.013	−1.5860	0.11
4d (^{4}F^e) – 3p (^{4}D^o)	188.5	A	1.443	−0.871	−0.097	−0.027	−1.6721	0.11
		B	1.450	−0.880	−0.092	−0.023	−1.6826	0.09
4d (^{4}D^e) – 3p (^{4}P^o)	180.1	A	0.811	−0.853	−0.109	−0.029	−1.6039	0.12
		B	0.815	−0.871	−0.099	−0.022	−1.6220	0.06
4d (^{4}P^e) – 3p (^{4}D^o)	187.0	A	0.335	−0.840	−0.116	−0.033	−1.5907	0.12
		B	0.337	−0.861	−0.105	−0.025	−1.6115	0.05
4d (^{4}P^e) – 3p (^{4}S^o)	200.2	A	0.248	−0.840	−0.116	−0.033	−1.5910	0.12
		B	0.249	−0.860	−0.106	−0.025	−1.6110	0.06
4d (^{2}F^e) – 3p (^{2}D^o)	193.8	A	0.515	−0.863	−0.103	−0.028	−1.6681	0.11
		B	0.534	−0.874	−0.097	−0.023	−1.6770	0.08
4d (^{2}D^e) – 3p$'$ (^{2}P^o)	384.5	A	0.020	−0.777	−0.157	−0.045	−1.5523	0.16
		B	0.623	−0.800	−0.146	−0.034	−1.5658	0.07
4d (^{2}P^e) – 3p$'$ (^{2}P^o)	373.8	A	0.026	−0.826	−0.136	−0.021	−1.5717	0.11
		B	0.275	−0.849	−0.124	−0.013	−1.5858	0.11
4p (^{4}D^o) – 4s (^{4}P^e)	1080.9	A	3.101	−0.881	−0.085	−0.027	−1.6450	0.10
		B	3.120	−0.896	−0.077	−0.022	−1.6598	0.06

Table 5. continued

Transition	λ[nm]	Case	a	b	c	d	f	%
4p (^{4}P^o) – 4s (^{4}P^e)	1207.9	A	1.853	−0.864	−0.095	−0.029	−1.5872	0.12
		B	1.865	−0.886	−0.083	−0.021	−1.6092	0.05
4p (^{4}S^o) – 4s (^{4}P^e)	960.0	A	0.244	−0.855	−0.101	−0.033	−1.5833	0.12
		B	0.246	−0.877	−0.089	−0.025	−1.6052	0.06
4p (^{2}D^o) – 4s (^{2}P^e)	1150.7	A	1.339	−0.875	−0.089	−0.028	−1.6508	0.11
		B	1.690	−0.877	−0.091	−0.023	−1.6430	0.05
4p (^{2}P^o) – 4s (^{2}P^e)	938.2	A	0.102	−0.531	−0.200	−0.080	−0.9693	1.67
		B	0.532	−0.770	−0.150	−0.040	−1.4455	0.07
4p (^{2}S^o) – 4s (^{2}P^e)	1106.6	A	0.032	−0.890	−0.063	−0.028	−1.5327	0.17
		B	0.247	−0.859	−0.113	−0.012	−1.5707	0.12
4p (^{4}D^o) – 3d (^{4}F^e)	905.2	A	3.217	−0.881	−0.085	−0.027	−1.6449	0.11
		B	3.236	−0.895	−0.077	−0.022	−1.6593	0.06
4p (^{4}D^o) – 3d (^{4}D^e)	815.5	A	0.660	−0.881	−0.085	−0.027	−1.6448	0.10
		B	0.664	−0.895	−0.077	−0.022	−1.6592	0.07
4p (^{4}D^o) – 3d (^{4}P^e)	957.3	A	1.301	−0.881	−0.085	−0.027	−1.6449	0.10
		B	1.309	−0.895	−0.077	−0.022	−1.6596	0.06
4p (^{4}P^o) – 3d (^{4}D^e)	885.8	A	1.543	−0.864	−0.095	−0.029	−1.5870	0.12
		B	1.553	−0.887	−0.083	−0.021	−1.6094	0.05
4p (^{4}S^o) – 3d (^{4}P^e)	861.2	A	1.112	−0.855	−0.101	−0.032	−1.5837	0.12
		B	1.119	−0.877	−0.089	−0.024	−1.6054	0.05
4p (^{2}D^o) – 3d (^{2}F^e)	880.0	A	1.336	−0.875	−0.089	−0.028	−1.6508	0.11
		B	1.686	−0.877	−0.091	−0.023	−1.6430	0.06
4p (^{2}D^o) – 3d (^{2}D^e)	843.7	A	0.265	−0.875	−0.089	−0.028	−1.6508	0.11
		B	0.335	−0.877	−0.091	−0.023	−1.6431	0.06
4p (^{2}P^o) – 3d (^{2}D^e)	723.5	A	0.062	−0.531	−0.200	−0.080	−0.9693	1.67
		B	0.319	−0.769	−0.150	−0.040	−1.4455	0.07
4p (^{2}S^o) – 3d (^{2}P^e)	912.5	A	0.058	−0.890	−0.063	−0.028	−1.5326	0.17
		B	0.457	−0.859	−0.113	−0.012	−1.5706	0.12
4p (^{4}D^o) – 3s (^{4}P^e)	138.8	A	0.519	−0.881	−0.085	−0.027	−1.6450	0.10
		B	0.522	−0.895	−0.077	−0.022	−1.6592	0.06
4p (^{4}P^o) – 3s (^{4}P^e)	140.7	A	1.590	−0.864	−0.095	−0.029	−1.5873	0.11
		B	1.601	−0.886	−0.083	−0.021	−1.6092	0.05
4p (^{2}D^o) – 3s (^{2}P^e)	147.3	A	0.386	−0.876	−0.089	−0.028	−1.6510	0.12
		B	0.487	−0.877	−0.091	−0.023	−1.6428	0.06
4p (^{2}P^o) – 3s′ (^{2}D^e)	209.3	A	0.094	−0.531	−0.200	−0.080	−0.9693	1.67
		B	0.486	−0.769	−0.150	−0.040	−1.4454	0.07
4s (^{4}P^e) – 3p (^{4}D^o)	304.4	A	2.126	−0.881	−0.083	−0.028	−1.6390	0.11
		B	2.139	−0.898	−0.074	−0.022	−1.6559	0.06
4s (^{4}P^e) – 3p (^{4}P^o)	278.4	A	4.461	−0.881	−0.083	−0.028	−1.6391	0.10
		B	4.489	−0.897	−0.074	−0.022	−1.6556	0.06
4s (^{2}P^e) – 3p (^{2}D^o)	309.5	A	0.244	−0.831	−0.108	−0.043	−1.5646	0.19
		B	1.487	−0.841	−0.113	−0.028	−1.5650	0.03
4s (^{2}P^e) – 3p (^{2}P^o)	341.1	A	0.203	−0.831	−0.108	−0.043	−1.5648	0.19
		B	1.235	−0.840	−0.113	−0.029	−1.5647	0.04
3d (^{4}F^e) – 3p (^{4}D^o)	322.0	A	22.958	−0.871	−0.098	−0.030	−1.7892	0.13
		B	23.110	−0.870	−0.098	−0.031	−1.7909	0.14
3d (^{4}D^e) – 3p (^{4}D^o)	335.2	A	3.610	−0.872	−0.097	−0.027	−1.7496	0.11
		B	3.634	−0.876	−0.094	−0.026	−1.7557	0.11
3d (^{4}D^e) – 3p (^{4}P^o)	303.9	A	13.271	−0.872	−0.098	−0.027	−1.7492	0.11
		B	13.356	−0.876	−0.095	−0.026	−1.7553	0.11
3d (^{4}P^e) – 3p (^{4}D^o)	315.9	A	1.785	−0.859	−0.104	−0.030	−1.6920	0.11
		B	1.796	−0.869	−0.098	−0.026	−1.7036	0.08
3d (^{4}P^e) – 3p (^{4}P^o)	288.0	A	1.680	−0.859	−0.104	−0.030	−1.6921	0.11
		B	1.690	−0.869	−0.098	−0.026	−1.7036	0.08

Table 5. continued

Transition	λ[nm]	Case	a	b	c	d	f	%	
3d (^{4}P^e) – 3p (^{4}S^o)	355.9	A	4.965	−0.859	−0.104	−0.030	−1.6921	0.11	
		B	4.995	−0.869	−0.098	−0.026	−1.7034	0.08	
3d (^{2}F^e) – 3p (^{2}D^o)	337.5	A	11.069	−0.866	−0.102	−0.031	−1.7917	0.14	
		B	11.582	−0.868	−0.101	−0.030	−1.7878	0.13	
3d (^{2}D^e) – 3p (^{2}D^o)	343.1	A	0.143	−0.847	−0.117	−0.032	−1.7699	0.14	
		B	2.353	−0.854	−0.112	−0.028	−1.7618	0.10	
3d (^{2}D^e) – 3p (^{2}P^o)	382.4	A	0.305	−0.847	−0.117	−0.032	−1.7701	0.13	
		B	4.994	−0.855	−0.112	−0.028	−1.7621	0.10	
3d (^{2}P^e) – 3p (^{2}D^o)	329.1	A	0.038	−0.844	−0.120	−0.032	−1.7385	0.12	
		B	0.348	−0.857	−0.112	−0.025	−1.7230	0.06	
3d (^{2}P^e) – 3p (^{2}P^o)	365.1	A	0.112	−0.843	−0.120	−0.032	−1.7382	0.12	
		B	1.035	−0.858	−0.112	−0.024	−1.7233	0.06	
3d (^{2}P^e) – 3p (^{2}S^o)	347.2	A	0.284	−0.843	−0.120	−0.032	−1.7380	0.12	
		B	2.627	−0.857	−0.112	−0.025	−1.7232	0.06	
3p (^{4}D^o) – 3s (^{4}P^e)	333.7	A	34.481	−0.889	−0.080	−0.028	−1.7577	0.11	
		B	34.717	−0.893	−0.077	−0.027	−1.7630	0.11	
3p (^{4}P^o) – 3s (^{4}P^e)	371.7	A	21.734	−0.889	−0.079	−0.027	−1.7102	0.10	
		B	21.883	−0.898	−0.074	−0.024	−1.7205	0.08	
3p (^{4}S^o) – 3s (^{4}P^e)	298.3	A	5.457	−0.873	−0.090	−0.030	−1.6836	0.10	
		B	5.492	−0.884	−0.083	−0.026	−1.6964	0.07	
3p (^{2}D^o) – 3s (^{2}P^e)	371.3	A	12.711	−0.885	−0.082	−0.030	−1.7753	0.13	
		B	17.419	−0.885	−0.085	−0.026	−1.7555	0.09	
3p (^{2}P^o) – 3s (^{2}P^e)	334.2	A	1.259	−0.900	−0.055	−0.008	−1.4918	0.29	
		B	11.544	−0.391	−0.276	−0.119	−1.1313	1.10	
3p (^{2}S^o) – 3s (^{2}P^e)	350.7	A	0.404	−0.926	−0.038	−0.027	−1.6928	0.09	
		B	3.020	−0.873	−0.099	−0.021	−1.7067	0.02	
3d′ (^{2}G^e) – 3p′ (^{2}F^o)	322.8	A	0.450	−1.272	0.074	0.121	−1.5981	0.16	*
3d′ (^{2}F^e) – 3p′ (^{2}F^o)	309.5	A	0.242	−2.022	0.688	0.377	−2.1683	1.00	*
		B	0.283	−2.016	0.682	0.377	−2.1705	1.02	*
3d′ (^{2}F^e) – 3p′ (^{2}D^o)	340.6	A	0.402	−2.022	0.688	0.377	−2.1684	1.00	*
		B	0.469	−2.016	0.682	0.376	−2.1705	1.02	*
3d′ (^{2}D^e) – 3p′ (^{2}F^o)	313.8	A	0.002	−2.100	0.713	0.455	−2.1856	1.44	*
		B	0.012	−2.087	0.705	0.446	−2.1853	1.41	*
3d′ (^{2}D^e) – 3p′ (^{2}D^o)	345.8	A	0.230	−2.100	0.712	0.455	−2.1855	1.44	*
		B	1.383	−2.087	0.705	0.446	−2.1852	1.41	*
3d′ (^{2}D^e) – 3p′ (^{2}P^o)	334.4	A	0.052	−2.100	0.712	0.455	−2.1855	1.44	*
		B	0.311	−2.087	0.705	0.446	−2.1854	1.41	*
3d′ (^{2}P^e) – 3p′ (^{2}D^o)	354.1	A	0.037	−2.125	0.730	0.468	−2.2109	1.52	*
		B	0.355	−2.112	0.723	0.459	−2.2108	1.49	*
3d′ (^{2}P^e) – 3p′ (^{2}P^o)	342.2	A	0.097	−2.125	0.730	0.468	−2.2109	1.52	*
		B	0.923	−2.112	0.723	0.459	−2.2108	1.49	*
3d′ (^{2}S^e) – 3p′ (^{2}P^o)	337.1	A	0.027	−2.140	0.739	0.477	−2.2111	1.55	*
		B	0.384	−2.125	0.731	0.467	−2.2115	1.52	*
3p′ (^{2}P^o) – 3s (^{2}P^e)	192.1	A	0.207	−1.946	0.657	0.327	−2.1850	0.96	*
		B	1.228	−1.893	0.628	0.295	−2.2645	0.88	*
3p′ (^{2}F^o) – 3s′ (^{2}D^e)	357.1	A	1.316	−0.474	−0.438	−0.159	−0.6738	0.29	*
		B	1.680	−0.410	−0.447	−0.179	−0.6242	0.45	*
3p′ (^{2}D^o) – 3s′ (^{2}D^e)	323.1	A	0.979	−2.030	0.689	0.392	−2.1739	1.12	*
		B	2.809	−2.035	0.685	0.404	−2.1908	1.23	*
3p′ (^{2}P^o) – 3s′ (^{2}D^e)	333.7	A	0.400	−1.946	0.657	0.327	−2.1848	0.96	*
		B	2.374	−1.893	0.629	0.295	−2.2649	0.87	*
3p″ (^{2}P^o) – 3s″ (^{2}S^e)	348.0	A	2.010	−2.194	0.929	0.323	−2.8430	0.92	*
		B	2.237	−0.240	−0.654	−0.455	−0.9234	3.21	*
3s″ (^{2}S^e) – 3p (^{2}P^o)	444.9	A	0.002	−2.200	0.953	0.303	−2.8340	0.87	*
		B	2.705	−0.258	−0.608	−0.415	−0.9247	2.85	*

Table 6. The factors $b(J_i, J_f)$, defined by Eq.(10), and wavelengths λ (in air) for the strongest multiplets of Ne II

Transition	λ[nm]	$b(J_i, J_f)$
3d (^{4}F^e) – 3p (^{4}D^o)		
$^4F_{9/2}$ – $^4D_{7/2}$	321.8193	0.357
$^4F_{7/2}$ – $^4D_{7/2}$	320.8965	0.041
$^4F_{7/2}$ – $^4D_{5/2}$	324.4095	0.245
$^4F_{5/2}$ – $^4D_{7/2}$	315.4795	0.002
$^4F_{5/2}$ – $^4D_{5/2}$	318.8743	0.052
$^4F_{5/2}$ – $^4D_{3/2}$	321.4329	0.160
$^4F_{3/2}$ – $^4D_{5/2}$	317.3574	0.003
$^4F_{3/2}$ – $^4D_{3/2}$	319.8916	0.040
$^4F_{3/2}$ – $^4D_{1/2}$	321.3735	0.100
3d (^{4}D^e) – 3p (^{4}P^o)		
$^4D_{7/2}$ – $^4P_{5/2}$	303.4461	0.400
$^4D_{5/2}$ – $^4P_{5/2}$	302.7016	0.090
$^4D_{5/2}$ – $^4P_{3/2}$	304.7556	0.210
$^4D_{3/2}$ – $^4P_{5/2}$	301.7311	0.010
$^4D_{3/2}$ – $^4P_{3/2}$	303.7720	0.107
$^4D_{3/2}$ – $^4P_{1/2}$	305.4677	0.083
$^4D_{1/2}$ – $^4P_{3/2}$	302.8700	0.017
$^4D_{1/2}$ – $^4P_{1/2}$	304.5556	0.083
3d (^{2}F^e) – 3p (^{2}D^o)		
$^2F_{7/2}$ – $^2D_{5/2}$	336.7218	0.571
$^2F_{5/2}$ – $^2D_{5/2}$	333.0734	0.029
$^2F_{5/2}$ – $^2D_{3/2}$	338.8417	0.400
3p (^{4}D^o) – 3s (^{4}P^e)		
$^4D_{7/2}$ – $^4P_{5/2}$	333.4836	0.400
$^4D_{5/2}$ – $^4P_{5/2}$	329.7726	0.090
$^4D_{5/2}$ – $^4P_{3/2}$	335.5016	0.210
$^4D_{3/2}$ – $^4P_{5/2}$	327.0800	0.010
$^4D_{3/2}$ – $^4P_{3/2}$	332.7153	0.107
$^4D_{3/2}$ – $^4P_{1/2}$	336.0597	0.083
$^4D_{1/2}$ – $^4P_{3/2}$	331.1272	0.017
$^4D_{1/2}$ – $^4P_{1/2}$	334.4395	0.083
3p (^{4}P^o) – 3s (^{4}P^e)		
$^4P_{5/2}$ – $^4P_{5/2}$	369.4213	0.350
$^4P_{5/2}$ – $^4P_{3/2}$	376.6259	0.150
$^4P_{3/2}$ – $^4P_{5/2}$	366.4073	0.150
$^4P_{3/2}$ – $^4P_{3/2}$	373.4938	0.044
$^4P_{3/2}$ – $^4P_{1/2}$	377.7133	0.139
$^4P_{1/2}$ – $^4P_{3/2}$	370.9622	0.139
$^4P_{1/2}$ – $^4P_{1/2}$	375.1245	0.028
3p (^{2}D^o) – 3s (^{2}P^e)		
$^2D_{5/2}$ – $^2P_{3/2}$	371.3079	0.600
$^2D_{3/2}$ – $^2P_{3/2}$	364.3927	0.067
$^2D_{3/2}$ – $^2P_{1/2}$	372.7107	0.333

the recombining ion, $2s^22p^4$ ^{3}P in the case of Ne^{2+}, is populated. This is a reliable approximation in the case of astrophysical objects having relatively low electron density. In our case, there are two additional states $2s^22p^4$ ^{1}D and ^{1}S having energies 25 840.8 cm^{-1} and 55 750.6 cm^{-1} (see Persson et al. 1991) above ground state. In our photoionization calculation, we obtained partial cross-sections from the states of Ne^{2+} to the ground state $2s^22p^4$ ^{3}P and to the ^{1}D and ^{1}S states of the same configuration. These data enable us to obtain coefficients for direct recombination leading to series other than those of ^{3}P parentage.

We generalised the model for calculation of the population structure for Ne$^+$ described in Sect. 3.1 to include the three lowest terms of the Ne^{2+} ion. To determine the population numbers of these states, we used a model which included collisional excitation, collisional deexcitation and radiative decay among these three states. For temperatures of $T_e \leq 20\,000$ K and electron densities of $N_e \leq 10^6$ cm^{-3} we found the population of excited ^{1}D and ^{1}S states to be very small (a maximum of 0.6% for ^{1}D and 0.00045% for ^{1}S). The extension of the full recombination calculation from one with only the ground term populated to a more extended one did not cause any substantial changes in the effective recombination coefficients. In general, only very small changes ($\leq 0.5\%$) were detected for strong lines. Changes of up to 2% occured for some lines originating from states with ^{1}D parentage but these lines were weak. For this reason, we present data which include recombination only to the ground state of the Ne^{2+} ion. Nevertheless, the effects of population in excited states in Ne^{2+} ion could become significant when densities become higher.

4.4. Discussion

The calculations described here were carried out entirely in *LS*-coupling. The work of Persson (1971) indicates that *LS*-coupling is no longer a good approximation for f- and g- states of Ne$^+$, and that the states should be described by an alternative coupling scheme. A full treatment of the high l states also needs to recognise the fact that the ground term of Ne^{2+} comprises three levels, $^3P_2$, $^3P_1$ and $^3P_0$ and that the populations of the ^3P_J levels may well differ from those given by the Boltzmann distribution, so that a correct treatment of the recombination to the high l states will require intermediate coupling photoionization data and incorporation of the population distribution among the ^3P_J levels.

We therefore do not present any transitions with $l > 2$ even though sometimes such multiplets have relatively strong lines with $\alpha_{eff} > 10^{-14}$ cm^3 s^{-1}. These transitions will be the subject of a subsequent paper.

Examining the data in Tables 3 and 4, one can see that for transitions from the 4d doublet states, the strongest lines are those with a final principal quantum number $n = 4$, rather than $n = 3$ as one might expect. For the transitions from the upper states 4d (^{2}D) and (^{2}P), there

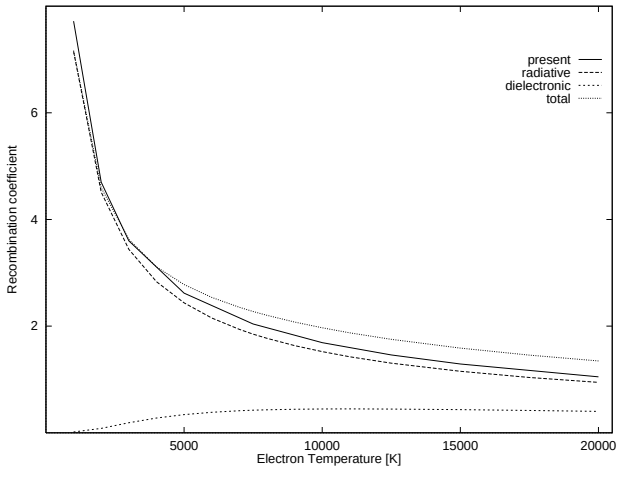

Fig. 2. Comparison of total recombination coefficients (in 10^{-12} cm^3 s^{-1}) for $Ne^{2+} + e^-$. The solid line represents the present calculation, the long-dashed line the radiative recombination coefficients of Péquignot et al. (1991), the short-dashed line the dielectronic recombination coefficients of Nussbaumer & Storey (1987). The dotted line is the sum of the radiative and dielectronic recombination coefficients

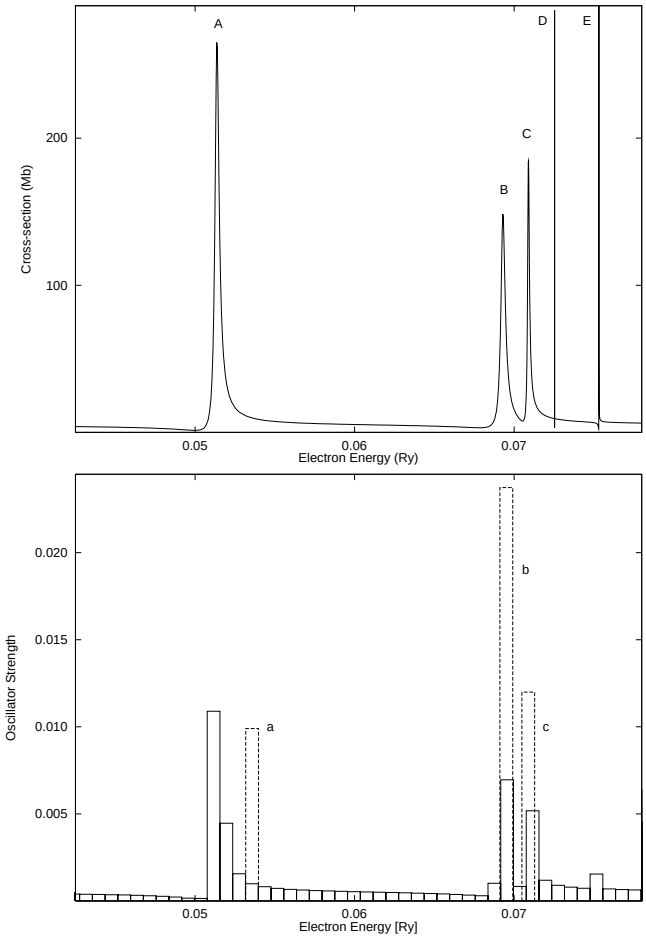

Fig. 3. Photoionization cross-section (in Mb) from the ground state $^2P^o$ of the Ne^+ ion (top) and oscillator strength distribution corresponding to the three lowest resonances obtained from these cross-section (solid line) and calculated by Nussbaumer & Storey (1987) (dashed line). In the top figure, the upper case letters denote transitions to the ground state from the doubly excited states: A – 3d$''$ ^{2}P, B – 5d$'$ ^{2}P, C – 5d$'$ ^{2}D, D – 5g$'$ ^{2}P, E – 5s$'$ ^{2}D. In the bottom figure, the lower case letters denote transitions from states: a – 3d$''$ ^{2}P, b – 5d$'$ ^{2}P, c – 5d$'$ ^{2}D

are no lines in the Tables terminating in a 3p state whereas lines terminating in 3p$'$ state are present. A similar situation was observed by Storey (1994) in the O II case. Closer examination of energy levels and oscillator strengths for these cases indicates that there exists a strong interaction between 3d$'$ states and the 4d levels of main series. This interaction redistributes the oscillator strength leading to weakness of the 4d–3p lines.

The present results for the total recombination coefficients (Table 2) can be compared with the radiative recombination coefficients (RR) for Ne II given by Péquignot et al. (1991), and the dielectronic recombination (DR) coefficients from Nussbaumer & Storey (1987). The comparison is shown in Fig. 2, which also shows the sum of the RR and DR results. The difference between our data and the sum of the RR and DR coefficients increases with temperature while the difference between our data and the RR coefficient decreases. This is due to the different temperature behaviour and different magnitude of the dielectronic component of the recombination coefficients that is obtained in the present work.

We cannot separate the radiative and dielectronic part of the total recombination coefficient in our method, so instead we consider the DR coefficients for the ground state $2s^22p^5$ ($^2P^o$) obtained in our work with those of Nussbaumer & Storey (1987), as a means of examining the importance of the resonance contributions to the recombination. In Fig. 3, we show a part of the photoionization cross-section for this state including the five lowest resonances. In the same figure we give the oscillator strength between the ground state and the continuum, binned into equal energy intervals, from the present photoionization data and from the work of Nussbaumer & Storey (1987). In the method of Nussbaumer & Storey (1987), resonances are treated as bound states and have no energy width, so we assign the oscillator strength in a particular resonance to one energy bin.

There are significant differences in resonance positions (especially for the first resonance) and oscillator strengths between the two sets of data. Our resonance A representing state 3d$''$ ^{2}P is closer to the ionization threshold and has a larger f-value than the corresponding resonance a of Nussbaumer & Storey (1987). This causes a more rapid rise and a larger value of the dielectronic component of the recombination compared to the DR data of Nussbaumer & Storey (1987). In Fig. 4 we show the recombination coefficients derived from these oscillator strength data. The relative positions of other resonances a rising from the

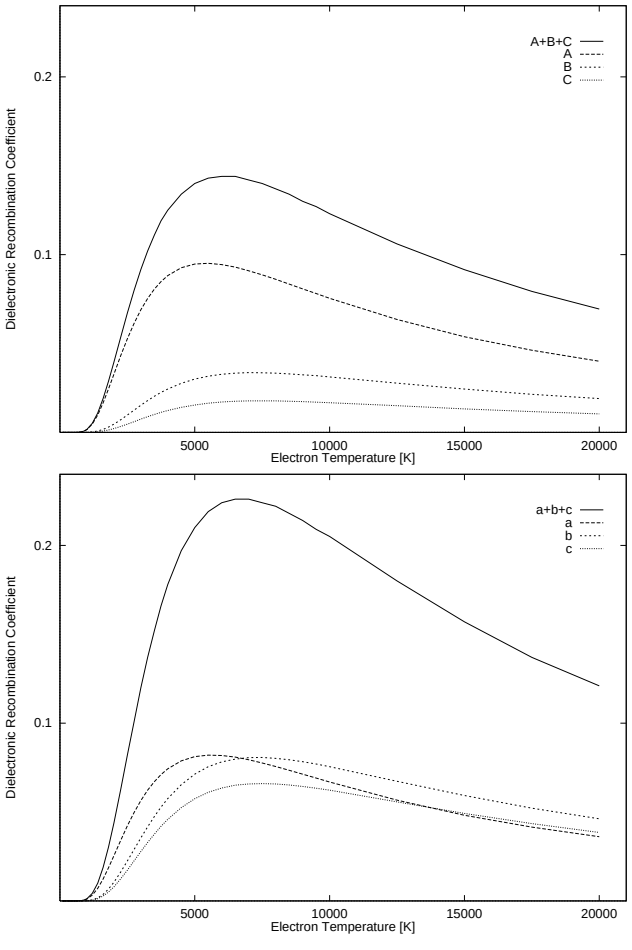

Fig. 4. Calculated coefficients (in 10^{-12} cm^3 s^{-1}) of dielectronic recombination (DR) to the ground state ^{2}P^o of Ne$^+$. The top figure shows DR coefficients obtained from the present data corresponding to the A, B, and C transitions of Fig. 3 and their total (solid line). The bottom figure shows DR coefficients obtained using data from Nussbaumer & Storey (1987) and corresponding to the a, b, and c transitions of Fig. 3 and their total (solid line)

series $2s^22p^4$ (^{1}D)nl are similar although the corresponding oscillator strengths are several time smaller in our calculation. For this reason the dielectronic contributions arising from these resonances are significantly larger in the Nussbaumer & Storey (1987) calculation (see lines B, C and b, c in Fig. 4). These three resonances contribute 50% of the total DR coefficient to the ground state, with the remainder coming from higher resonances and cascading from upper states. We conclude from these comparisons that there are significant differences in resonance positions and areas between the present results and those of Nussbaumer & Storey (1987), and that in our calculation the dielectronic component is significantly smaller than in that work. We believe the current work to be significantly more accurate than that of Nussbaumer & Storey (1987).

5. Conclusion

Total recombination coefficients for Ne$^+$ ions and effective recombination coefficients for lines of Ne II have been tabulated at temperatures and densities appropriate to nebular plasmas. The use of atomic data of high quality for bound-bound and bound-free radiative processes among all the terms with $n \leq 15$ means that the results given here should be more reliable than those of previous workers. It would be desirable to extend the calculations to higher electron densities to permit reliable interpretation of Ne II emission from more dense objects such as young novae and stellar winds.

In Ne II itself, further work is needed on the transition arrays where LS-coupling breaks down. Relatively strong recombination lines exist between 5g, 4f and 3d states which cannot be reliably used at present.

References

Baker J.G., Menzel D.H., 1938, ApJ 88, 52
Bates D.R., Damgaard A., 1949, Phil. Trans. A. 242, 101
Bell R.H., Seaton M.J., 1985, J. Phys. B. 18, 1589
Berrington K.A., Burke P.G., Butler K., Seaton M.J., Storey P.J., Taylor K.T., Yu Yan, 1987, J. Phys. B 20, 6379
Brink D.M., Satchler G.R., 1968, "Angular Momentum". Oxford University Press
Burgess A., Seaton M.J., 1960, MNRAS 120, 121
Burgess A., 1964, ApJ 139, 776
Cunto W., Mendoza W., Ochsenbein F., Zeippen C.J., 1993, A&A 275, L5
Eissner W., Jones M., Nussbaumer H., 1974, Computer Phys. Commun. 15, 23
Gordon W., 1929, Ann. Phys. (Leipzig) 5(2), 1031
Hummer D.G., Berrington K.A., Eissner W., Pradhan A.K., Saraph H.E., Tully J.A., 1993, A&A 279, 298
Hummer D.G., Storey P.J., 1987, MNRAS 224, 801
Hummer D.G., Storey P.J., 1992, MNRAS 254, 277
Liu X.-W., Storey P.J., Barlow M.J., Clegg R.E.S., 1995, MNRAS 272, 369
Nussbaumer H., Storey P.J., 1978, A&A 64, 139
Nussbaumer H., Storey P.J., 1983, A&A 126, 75
Nussbaumer H., Storey P.J., 1984, A&A 56, 293
Nussbaumer H., Storey P.J., 1987, A&AS 69, 123
Peach G., 1967, Mem. R. Astron. Soc. 71, 1
Péquignot D., Petitjean P., Boisson C., 1991, A&A 251, 680
Persson W., 1971, Phys. Scr. 3, 133
Persson W., Wahlström C.-G., Jönsson L., Di Rocco H.O., 1991, Phys. Rev. A 43, 4791
Seaton M.J., 1983, Rep. Prog. Phys. 46, 167
Seaton M.J., 1987, J. Phys. B 20, 6363
Seaton M.J., Storey P.J., 1976, Atomic processes and applications, Burke P.G. and Moiseiwitsch B.L. (eds.), North Holland, p. 134
Storey P.J., Hummer D.G., 1991, Computer Phys. Commun. 66, 129
Storey P.J., 1994, A&A 282, 999
van Regemorter H., Dy H.B., Prud'homme M., 1979, J. Phys. B 12, 1053